ACS Catalysis

pubs.acs.org/acscatalysis
Research Article

Unraveling the Oxidation Mechanism of Formic Acid on Pd(111) Electrode: Implication from pH Effect and H/D Kinetic Isotope Effect

Zhen Wei,[§] Meng-Ke Zhang,[§] Yan-Hao Yu, Jun Cai, Yan-Xia Chen,* Juan M. Feliu, and Enrique Herrero*

Cite This: *ACS Catal.* 2024, 14, 8983−8995

ABSTRACT: The pH effect and H/D kinetic isotope effect (KIE) of formic acid oxidation reaction (FAOR) on Pd(111) have been systematically investigated by cyclic voltammetry. In addition, the pH effect of acetate adsorption on Pd(111) is also studied to have a deep understanding of the role of adsorbates on Pd(111) during the FAOR process. The results clearly show: (1) In solutions with a fixed concentration of acetic acid, the onset potential of acetate desorption is almost unchanged on the reversible hydrogen electrode (RHE) scale with the increase of pH when the pH is lower than the pK_a of acetic acid. However, when the pH is higher than the pK_a of acetic acid, the onset potential of acetate desorption shifts positively with a slope of ca. 20 mV per pH unit; (2) In solutions with pH less than 6, the maximum coverage of acetate adsorbed on the Pd(111) electrode is about 0.26 ML; (3) In acidic solutions, FAOR on Pd(111) has obvious pH effect in the potential range of current increasing on SHE scale. After correcting the pH^s-induced shift, the onset potential of FAOR shifts negatively by ca. 90 mV per pH unit. However, the pH effect disappears in the potential range after the peak; (4) In alkaline solutions, the onset potential of FAOR is influenced by OH_{ad}; (5) The H/D KIE factor of FAOR on Pd(111) is ca. 5 in the pH range of 1−14. Two possible mechanisms trying to explain these results have been proposed. In one, $COO_{ad}^{\lambda-}$ is the active intermediate and the formation of this intermediate is the rate-determining step (RDS), whereas, in the second one, monodentate adsorbed formate ($HCOO_m$) is the active intermediate and its dissociation on the surface is the RDS. The simulated results with both mechanisms are compared with the experimental results and discussed critically.

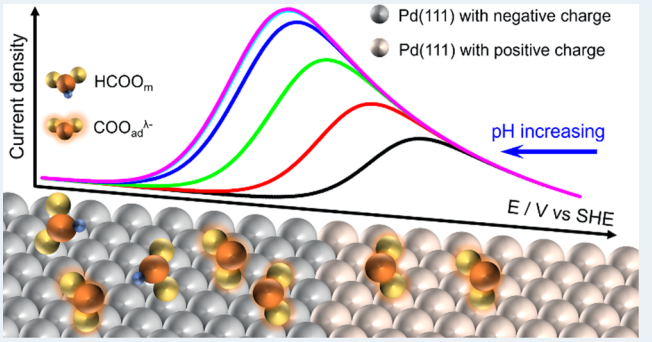

KEYWORDS: *Pd(111), formic acid oxidation, acetate adsorption, pH effect, H/D KIE*

1. INTRODUCTION

Cleaner energy based on the oxidation of small organic molecules has been regarded as a prospective source to reduce the dependence on traditional fossil fuels.[1−7] The formic acid oxidation reaction (FAOR) is the simplest oxidation reaction among those of small organic molecules because it exchanges only two electrons. In addition, formate is also an intermediate product in the oxidation reaction of other small organic molecules. Based on these facts, FAOR is considered one of the most important model reactions in electrocatalysis, which can pave the way for understanding the reaction mechanisms of oxidation reaction involving the transfer of several electrons.[8−10]

Platinum and palladium surfaces are effective in activating the C−H bond cleavage,[11] giving rise to lower overpotentials for the oxidation of small organic molecules than those observed on other metals, such as gold.[8,12] A lot of efforts have been made in the past to elucidate the reaction mechanism of FAOR on Pt.[9,10,12,13] It is widely accepted that the FAOR on Pt electrodes presents a dual pathway mechanism with a direct pathway, which is the main contribution to the measured currents for the FAOR, and an indirect pathway, which forms adsorbed CO at low potentials blocking the surface and preventing subsequent oxidation of formic acid.[13] The undesired indirect reaction pathway results in Pt not being an ideal choice for addressing fundamental questions, especially for unraveling the mechanism of the direct pathway for FAOR.

In contrast to Pt electrodes, on the Pd electrode, the undesired indirect reaction pathway generating CO is suppressed, which makes Pd an ideal choice to study the mechanism of the direct pathway for FAOR without the interference of CO poisoning.[14−16] More importantly, the

Received: April 6, 2024
Revised: May 7, 2024
Accepted: May 13, 2024

https://doi.org/10.1021/acscatal.4c02040
ACS Catal. 2024, 14, 8983−8995

activity of FAOR on the Pd electrode is also high, turning Pd-based catalysts into a promising electrocatalyst for small organic molecule fuel cells.[17,18] A mechanistic study of FAOR on Pd by surface-enhanced infrared absorption spectroscopy in the attenuated total reflection mode (ATR-SEIRAS) shows that the poisoning of the Pd surface by CO is very slow and scarcely affects the FAOR. In addition, adsorbed formate is detected only when formic acid oxidation is suppressed.[19]

Compared to Pd-based catalysts, Pd single-crystal electrodes are more suitable for studying the mechanism of FAOR because of the defined and simple surface structure of the electrode. However, because Pd single-crystal electrodes are difficult to prepare, there have been few studies for FAOR on Pd single-crystal electrodes in the past.[20,21] Hoshi et al. found that, on the low-index planes of Pd, the maximum current density of FAOR increases in the positive scan direction as follows: Pd(110) < Pd(111) < Pd(100), which differs from that on the low-index planes of Pt: Pt(111) < Pt(110) < Pt(100). In addition, Pd(111) and Pd(110) showed a very significant FAOR activity at ca. 0.2 V_{RHE}.[20] Due to the difficulties of preparing with Pd single-crystal electrodes, epitaxially grown Pd layers on a foreign metal are regarded as an alternative method to explore the behavior of FAOR on Pd.[1,22−24] Kolb et al. found that when compared to the massive Pd single-crystal surfaces, the electrocatalytic properties of the Pd overlayers depended markedly on their thickness and crystallographic orientation.[24] A study on the FAOR at Pd-modified Pt(100) and Pt(111) by a combination of voltammetry and differential electrochemical mass spectrometry (DEMS) allowed a better understanding of the reaction taking place on the electrode surface. It is shown that on Pd-modified Pt(100) electrodes and in the potential region below 0.3 V, the currents in the positive scan direction are higher than those recorded in the negative-going scan. The lower currents in the negative scan direction are due to the CO_2 reduction to CO taking place on the border of the Pd islands.[22] Recently, Koper et al. investigated the reason for the absence of the indirect pathway during FAOR on the Pd electrode. Based on the (high-scan-rate) cyclic voltammetry (CV) and density functional theory (DFT) calculations, they suggested the coverage of bidentate adsorbed formate ($HCOO_b$) is higher on Pd_{ML}-Pt(111) than that on bare Pt(111).[1] As a result, there are not enough free active sites on the Pd_{ML}-Pt(111) surface for generating CO (the occurrence of the CO pathway requires two or more adjacent free sites at the same time), which blocks the CO pathway and protects the electrode surface.[1] Due to the affinity of the Pd surface to hydrogen, formate is more likely adsorbed with C−H down configuration toward the Pd surface and promotes the activity of FAOR.[1]

However, the behavior of FAOR on the thin layer of Pd is different from that on massive Pd electrodes due to the strong electronic effect from the substrate. For example, the $HCOO_b$ signal cannot be detected by ATR-SEIRAS in the main potential range for the FAOR on the Pd electrode.[19] On the other hand, the $HCOO_b$ signal during the FAOR on Pd_{ML}-Pt(111) can be detected by fast scan voltammetry.[1] In addition, the kinetics of the FAOR on massive Pd electrode may be affected by hydrogen absorption at low potential.[25,26] Based on these facts, using the epitaxial Pd_{ML}-Pt(111) electrode (or Pd_{ML}-Au(111)) to study the mechanism of FAOR on massive Pd electrodes is not the best choice.

To unravel the exact mechanism for FAOR on Pd electrodes, the studies of the pH and H/D kinetic isotope effects (KIE) of the FAOR on the Pd(111) electrode were carried out. In addition, the acetate adsorption on the Pd(111) electrode is also studied to have a deeper understanding of the roles of adsorbates on Pd(111) during the FAOR process. Formate and acetate adsorb on the metal electrode surface mainly through the carboxylic group. Since acetate is inert in the stability range of the Pd single-crystal electrodes, it is possible to study its adsorption behavior without interference from any oxidation process. On the other hand, formic acid/formate is readily oxidized in the potential range where its adsorption takes place, and thus, determining its adsorption behavior under these circumstances is difficult. Owing to the similarities between acetate and formate in their adsorption behavior, the results of the acetate adsorption can be transferred to the formate adsorption. These studies will provide a deeper understanding of the mechanism of FAOR on the Pd(111) electrode.

2. EXPERIMENTAL SECTION

A bead-type Pd(111) electrode (diameter ca. 3 mm) is prepared from a Pd wire (0.8 mm diameter, 99.99% purity, Tanaka Noble Metal Corp.) according to Clavilier's technique.[27,28] In brief, the Pd wire is annealed using a H_2+O_2 flame until a seed crystal is formed. The crystal is melted and solidified several times until the dissolved gas does not explode on the surface. After cooling, the resulting single crystal bead is oriented, cut, and polished to obtain the desired (111) surface orientation. The obtained Pd(111) electrode is then annealed by inductive heating equipment (Easyheat 244, Ambrell Companies) at about 1300 °C in an argon atmosphere (99.9999%), cooled down for 1 min in a stream of argon, and then quenched in ultrapure water that is in equilibrium with the Ar atmosphere before any voltammetric measurement. The electrode surface is protected with a deoxygenated water droplet to prevent any contamination during its transfer to the electrochemical cell. A meniscus between the Pd(111) surface and the electrolyte is formed while the potential is held at 0.5 V (vs reversible hydrogen electrode, RHE). A conventional two-compartment, three-electrode glass cell was used for all of the electrochemical measurements, in which the reference and working electrode are located in two compartments separated by a long capillary. A Ag/AgCl electrode and a Pd foil electrode were used as reference electrode (RE) and counter electrode (CE), respectively. Careful control experiments confirm that after 5 h of measurements, the solutions are not contaminated by Cl^-. The electrode potentials were controlled by a potentiostat (Autolab 302N).

The electrolyte solutions with 0.1 M HCOOH or DCOOH + 0.1 M $HClO_4$ + x M KOH (x = 0−0.285) and 0.1 M $HClO_4$ + 0.1 M CH_3COOH + y M KOH (y < 0.2), whose pH values are in the range from 1 to 13. These solutions were prepared with perchloric acid (70%, Suprapure, Sigma-Aldrich), formic acid (HCOOH, 98%, Suprapure, Sigma-Aldrich or DCOOH, 98%, Suprapure, Sigma-Aldrich), KOH (99.99%, Suprapure, Sigma-Aldrich), CH_3COOH (99.99%, Suprapure, Sigma-Aldrich) and ultrapure water (18.2 MΩ cm). Before each experiment, all solutions were purged with Ar (99.999%, the Linde Group, China) for 20 min. Then, the blank cyclic voltammogram (CV) for Pd(111) in 0.1 M H_2SO_4 was recorded to ensure that the CV showed the well-documented features for the Pd(111) electrode, confirming that the

https://doi.org/10.1021/acscatal.4c02040
ACS Catal. 2024, 14, 8983−8995

homemade Pd(111) electrode is well ordered and the cell system used for the study is clean. The formic acid oxidation reaction was studied using the hanging meniscus rotating disk electrode (HMRDE) at a rotating rate of 1000 rpm. The HMRDE was controlled using a modulated rotator (Hokuto Denko Ltd.). During all of the electrochemical measurements, the atmosphere in the cell above the electrolyte was purged continuously with Ar. All experiments were carried out at about 25 °C and with 95% compensation of the ohmic drop. The detailed model of correction of the FAOR-induced drift of the interfacial pH (pH^s) is given in ref 29, which is also briefly described in the Supporting Information (SI).

3. RESULTS AND DISCUSSION

3.1. Experiment Results. *3.1.1. The Behavior of FAOR on Pd(111).* Figure 1a shows the cyclic voltammogram for

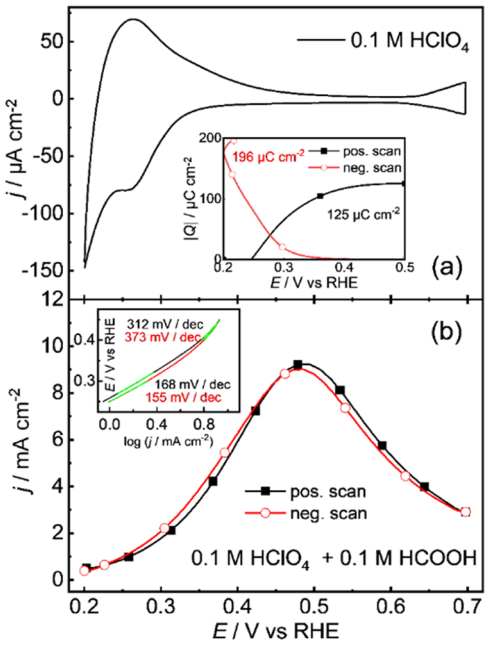

Figure 1. Cyclic voltammograms for Pd(111) in (a) 0.1 M $HClO_4$ and (b) 0.1 M $HClO_4$ + 0.1 M HCOOH in the positive (black line) and negative (red line) scan directions. Scan rate: 50 mV/s. Rotation rate: 1000 rpm. Inset in (a): the integrated anodic charge for the $j-E$ curve in the positive scan direction (from 0.22 to 0.5 V) and the cathodic charge for the $j-E$ curve in the negative scan direction (from 0.5 to 0.2 V and back to 0.22 V). Inset in (b): the corresponding Tafel plot for FAOR at Pd(111).

Pd(111) at 0.1 M $HClO_4$. Obviously, the basic CV of Pd(111) in solution without strongly adsorbed anions has a remarkable hydrogen adsorption region (0.2−0.38 V) and OH_{ad} adsorption region (0.6−0.7 V). When the electrode potential is negatively scanned to E < 0.38 V, the cathodic current which is related to the underpotential deposition of H (H_{UPD}) on Pd(111) and the absorption of H (H_{abs}) into the Pd crystal gradually increases. The small peak at ca. 0.3 V can be preliminarily attributed to hydrogen absorption, which is superimposed on a broad $j-E$ curve related to hydrogen adsorption.[15,30] In the positive scan from 0.22 to 0.4 V, significant anodic currents due to the removal of surface H_{UPD} and H_{abs} from the interior of the Pd lattice can be detected. After correcting the apparent double-layer charging current, the integrated cathodic charge in the potential from 0.5 to 0.2 V and then back to 0.22 V (where current reaches 0 value in the positive scan direction) is ca. 196 $\mu C\ cm^{-2}$, while the integrated anodic charge from 0.22 to 0.5 V is only ca. 125 $\mu C\ cm^{-2}$, as shown in the inset of Figure 1a. This charge difference indicates that a significant amount of H absorbed in the previous negative scan direction cannot be removed in the subsequent positive scan. At around 0.7 V, a pair of symmetric redox peaks can be observed, which are assigned to OH_{ad} produced by water decomposition. It should be noted that when the potential is too high, irreversible oxidation and/or dissolution of Pd occurs.[31,32] Therefore, in order to avoid the destruction of the ordered structure of the Pd single crystal, the low and high potential limits are set at 0.2 and 0.7 V, respectively.

Figure 1b displays the FAOR behavior of Pd(111) in 0.1 M $HClO_4$ + 0.1 M HCOOH. The FAOR currents in the positive and negative scan directions are almost identical, indicating no CO is generated during the FAOR process. FAOR on Pd(111) starts at E < 0.2 V. With the increase of potential, FAOR currents rise and then reach a maximum value at ca. 0.5 V. The increase of the FAOR current from 0.2 to 0.5 V can be rationalized by the increase of overpotential (driving force), which is consistent with the prediction of the Bulter-Volmer (BV) equation. However, when E > 0.5 V, the FAOR currents begin to decrease, which is in contrast to the prediction by the BV theory. As has been proposed previously,[8] some adsorbates on the Pd(111) surface during the FAOR process give rise to the current drop at E > 0.5 V. Compared with Figure 1a, the peak potential (0.5 V) for the FAOR is ca. 0.1 V more negative than the onset potential for OH_{ad} adsorption on Pd(111). In addition, Osawa et al. suggested the onset potential of the Pd surface oxidation in a solution containing formic acid is 0.15 V more positive than that observed in the electrolyte free of HCOOH.[19] Very similar behavior also has been observed in the oxidation of formic acid[33] and formaldehyde[34,35] on Pt. All of these facts indicate that the drop in the FAOR is not due to the poison from O/OH on the Pd(111) surface. Additionally, although the FAOR on the Pd(111) electrode produces a large amount of CO_2, in the RDE configuration, the produced CO_2 is readily transferred from the electrode surface to the bulk solution so that the poisoning effect from the CO_2 reduction to CO can be ignored.[36] According to the ATR-SEIRAS, bidentate adsorbed formate cannot be detected in the potential region before FAOR peak potential, and can only be observed when formic acid oxidation is suppressed.[19] On one hand, this fact indicates that $HCOO_b$ is not the active intermediate. On the other hand, because $HCOO_b$ appeared at the turning point of the trend of the $j-E$ curve of FAOR, it is reasonable to assume that this species is a poison for the FAOR on the Pd electrode.

The Tafel slope for FAOR on Pd(111) in the potential region below 0.3 V is ca. 150 ± 10 mV and increases to ca. 340 ± 30 mV at 0.5 V, as shown in the inset of Figure 1b. The high Tafel slope of FAOR on Pd(111) in the lower-potential region has been explained as an effect of H absorption. With the increasing electrode potential from 0.2 to 0.3 V, the amount of absorbed H decreases, and as a result, the enhancement of the FAOR kinetics also decreases. This effect is superimposed with the enhancement of kinetics by the increase of the overpotential, which leads to a large Tafel slope between 0.2 and 0.3 V.[25]

3.1.2. pH Effect of Acetate Adsorption on Pd(111). In order to verify the hypothesis mentioned above regarding

https://doi.org/10.1021/acscatal.4c02040
ACS Catal. 2024, 14, 8983−8995

$HCOO_b$ and to determine the potential region for its adsorption on Pd(111), fast scan voltammetry, a common method to measure the adsorption behavior of intermediates during electrocatalytic reactions, was carried out. However, this effort has been found to be in vain (Figure S1), owing to the large oxidation currents. Because acetate is adsorbed on the Pd surface through the carboxylic acid in a bidentate configuration in a similar way to $HCOO_b$,[37] the current wave for acetate adsorption on Pd(111) can provide insights into the behavior of $HCOO_b$ and the role of adsorbed species in the FAOR.

Figure 2 shows a representative CV of Pd(111) in 0.1 M $HClO_4$ + 0.1 M CH_3COOH recorded at a scan rate of 10 mV/s. For comparison, the basic CV of Pd(111) in 0.1 M $HClO_4$ with the same scan rate is also included. In the presence of acetate anions, hydrogen adsorption on Pd(111) starts around 0.33 V, ca. 30 mV more negative than that in 0.1 M $HClO_4$, which is the result of the inhibition of hydrogen adsorption due to the strong adsorption of CH_3COO_b on Pd(111). Analogously to what is observed with (bi)sulfate adsorption,[15,30] the sharp cathodic peak at ca. 0.26 V is attributed to the desorption of acetate, which is accompanied by the hydrogen adsorption onto Pd(111) and absorption of hydrogen into the Pd crystal. The corresponding anodic peak appears at ca. 0.28 V, evidencing the superposition of hydrogen desorption and acetate adsorption processes. At the same time, the formation of OH_{ad} is inhibited due to the adsorption of acetate, which is consistent with the observations on Pt(111).[37] Figure 2 reveals that, on Pd(111), the thermodynamic equilibrium potential for the formation/removal of H_{UPD} and the desorption/adsorption of acetate are in the same potential region, leading to a competition of hydrogen and acetate for the surface sites at these potentials. The inset of Figure 2 shows the integrated anodic charge for the j–E curves in the positive scan direction (from 0.22 to 0.5 V) and the cathodic charge (from 0.5 to 0.2 V and back to 0.22 V). It is found that in the potential region below 0.31 V, the difference of anodic (or cathodic) charge recorded in the presence and absence of acetic acid in solution is ca. 64 μC cm^{-2}. This may be roughly taken as the pseudocapacitive charge flow due to acetate adsorption, assuming that the amount of H being adsorbed/absorbed is not significantly affected due to the completion of acetate adsorption. Taking into account that a theoretical charge density of 246 μC cm^{-2} should flow through the circuit for the formation of 1 ML of hydrogen (1 electron per Pd surface atom), the maximum acetate coverage at Pd(111) is ca. 0.26 ML, which is nearly the same as that of $HCOO_b$ on Au(111)[8] and Pt(111).[1]

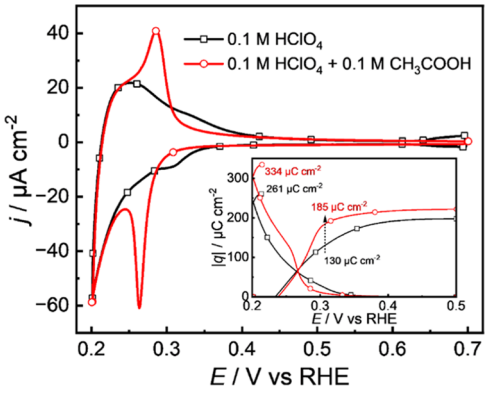

Figure 2. Cyclic voltammograms of Pd(111) electrode in 0.1 M $HClO_4$ (black line) and 0.1 M $HClO_4$ + 0.1 M CH_3COOH (red line). Scan rate: 10 mV/s. The inset shows the integrated anodic charge for the j–E curve (from 0.22 to 0.5 V) and the cathodic charge for the j–E curve (from 0.5 to 0.2 V and back to 0.22 V).

In order to collect more information on acetate adsorption, a study of the pH effect on acetate adsorption was carried out. Figure 3 displays the CVs of Pd(111) in 0.1 M $HClO_4$ + 0.1 M CH_3COOH + x M KOH (x < 0.2). It is clear that, when the overall concentration of acetic acid/acetate is fixed, the peak of the current wave in the H-UPD region shifts positively in the RHE scale with the increase of pH. As shown in the inset of Figure 3, the difference between the integrated anodic charge for the j–E curves (from 0.22 to 0.5 V) and the cathodic charge (from 0.5 to 0.2 V and back to 0.22 V) is nearly the same, unlike what is observed in solutions with low buffer capacity.[30] In the latter type of solutions, the difference between the integrated anodic charge (from 0.22 to 0.5 V) and the cathodic charge (from 0.5 to 0.2 V and back to 0.22 V) for the j–E curves gradually decreases with increasing pH.[30] These differences can be explained by changes in the interfacial pH. In solutions with a low buffer capacity, at pH > 3, there are not enough hydrogen ions in solutions to satisfy the needs of hydrogen absorption and hydrogen adsorption at the same time, increasing the interfacial pH and, consequently, leading to weaker hydrogen absorption. However, for solutions with pH > 3 in the presence of acetic acid, even if hydrogen ions in the solution are insufficient, acetic acid molecules can also be used as a proton source to release H^+, since the pK_a of acetic acid is 4.76. Thus, the hydrogen demand for the absorption reaction is met and the interfacial pH is maintained, resulting in an almost constant difference between the integrated anodic and cathodic charges. In addition, as Figure S2 shows, with the increase in pH, the maximum coverage of acetate adsorbed on the electrode surface remains unchanged at about 0.26 ML. Clearly, because of the high amount of supporting electrolyte and the good buffer capacity of acetic acid at the pH value around its pK_a, higher peak currents in the H-UPD region in this pH in the positive scan direction are observed.

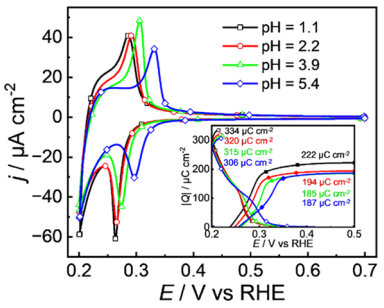

Figure 3. CVs of the Pd(111) electrode in 0.1 M $HClO_4$ + 0.1 M CH_3COOH + x M KOH (x < 0.2), scan rate: 10 mV/s. Inset: the integrated anodic charge (from 0.22 to 0.5 V) and the cathodic charge (from 0.5 to 0.2 V and back to 0.22 V) for the j–E curves.

The pH dependence of the potential of the peak in the H-UPD region and the onset potential for acetate desorption in the RHE scale is plotted in Figure 4a. The onset potential for acetate desorption is defined when the cathodic current density is ca. −2 μA cm^{-2} (the current density for the double-layer charging is ca. ± 0.5 μA cm^{-2}). Here, the pH dependence is also shown in the SHE scale to facilitate subsequent formic

https://doi.org/10.1021/acscatal.4c02040
ACS Catal. 2024, 14, 8983−8995

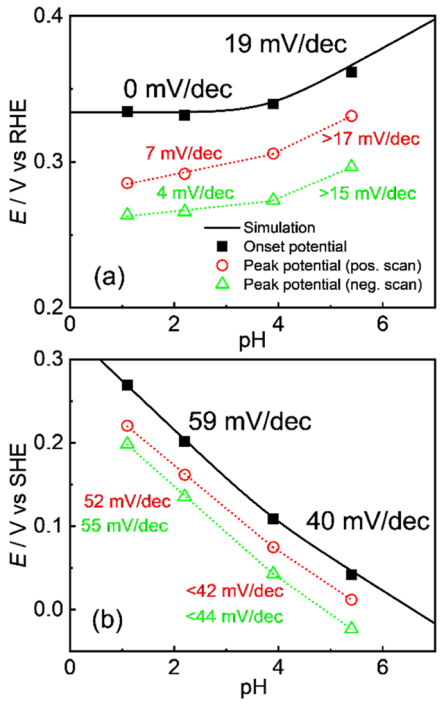

Figure 4. Peak potential of the current wave in the H-UPD region and the onset potential of acetate desorption as a function of the solution pH in (a) RHE scale and (b) SHE scale.

acid oxidation analysis, as shown in Figure 4b. As expected, in the RHE scale, the onset potential for acetate desorption is nearly constant when the pH is lower than the pK_a of acetic acid. When the pH is higher than pK_a, the onset potential of acetate desorption shifts positively with a slope of ca. 19 mV. In addition, the E_{peak} vs pH has slopes of ca. 5 mV when the pH < pK_a of acetic acid, and they increase to ca. 16 mV when the pH is higher than pK_a.

In the following, an explanation for the pH-dependent adsorption of acetate is provided. Similar to the adsorption of $HCOO_b$,[8] the adsorption of acetate may have the acetic acid molecule or the acetate ion as a precursor.[26] In addition, it should be noted that, in solutions with high proton concentration, acetate adsorption occurs in parallel with the desorption of H_{ad} in the same potential range. Acetate is adsorbed on the Pd surface through the carboxylic acid in a bidentate configuration, which is similar to that found on Pt(111) and Au(111).[37,38] Therefore, it can be assumed that one acetate ion displaces two H_{ad} atoms and the overall reaction can be written as

$$CH_3COOH + 2H_{ad} \rightleftarrows CH_3COO_b + 3H^+ + 3e^- \quad \text{(R-1)}$$

$$CH_3COO^- + 2H_{ad} \rightleftarrows CH_3COO_b + 2H^+ + 3e^- \quad \text{(R-2)}$$

For the adsorption of acetate, its adsorption process should be faster than the desorption process, due to the disturbance of the desorption process brought by absorbed hydrogen. As an approximation, both R-1 and R-2 can be viewed to be in fast quasi-equilibrium. Meanwhile, the dissociation of acetic acid is also very fast so that acetic acid and acetate ions can be approximated to be in equilibrium near the interface. In this case, the adsorption behaviors of R-1 and R-2 are the same, because the concentrations at the interphase of acetic acid (c^s_{HAC}) and acetate ($c^s_{AC^-}$) are linked by the acid constant, K_a. Taking R-1 as an example, its thermodynamic equilibrium potential (E_{eq} vs RHE) is

$$E^1_{eq} = E^0_1 + \frac{RT}{3F}\ln\frac{\theta_{AC_b} c_{H^+}{}^3}{c^s_{HAC}\theta_{H_{ad}}{}^2} + 0.059\ \text{pH}$$
$$= E^0_1 + \frac{RT}{3F}\ln\frac{\theta_{AC_b}}{\theta_{H_{ad}}{}^2} + \frac{RT}{3F}\ln\frac{c_{H^+}{}^3}{c^s_{HAC}} + 0.059\ \text{pH} \quad (1)$$

where E^0_1 is the standard equilibrium potential of reaction R-1, θ_{AC_b} and $\theta_{H_{ad}}$ are the coverages of acetate and hydrogen, respectively, and c_{H^+} is the proton concentration. When the thermodynamic equilibrium potential is under conditions where the coverages of adsorbates are the same, i.e., θ_{AC_b} and $\theta_{H_{ad}}$ have fixed values, eq 1 can be reformulated as

$$E^1_{eq} = E^{0'}_1 + \frac{RT}{3F}\ln\frac{c_{H^+}{}^3}{c^s_{HAC}} + 0.059\ \text{pH} \quad (2)$$

where $E^{0'}_1$ is equal to $E^0_1 + \frac{RT}{3F}\ln\frac{\theta_{AC_b}}{\theta_{H_{ad}}{}^2}$. From eq 2, it is obvious that when the electrode material and its surface structure are fixed, E^1_{eq} is just a function of solution composition, which is specified by our experiments. The result of the simulation of pH dependence of the equilibrium potential of acetate adsorption is shown in Figure 4 with a black line, which agrees well with the pH dependence of onset potential for acetate desorption observed experimentally. The onset potential is clearly a region where the assumptions made to reach eq 2 are reasonable. At the onset potential for acetate desorption, it is safe to assume that the θ_{AC_b} is the same (0.26 ML, Figure S2), while $\theta_{H_{ad}}$ is also the same and is close to zero. As a result, the tendency of the pH-dependent shift of onset potential of acetate desorption agrees well with the result of simulation from eq 2. On the other hand, since θ_{AC_b} and $\theta_{H_{ad}}$ are different at the peak potential for different pHs, experimental data do not agree with the model. For alkaline solutions, this onset potential will be more positive than that for OH_{ad}, and thus acetate adsorption will not take place.

3.1.3. pH Effect of FAOR on Pd(111). The solutions with (bi)phosphate are usually used to maintain the interfacial pH during the study of the pH effect of FAOR. However, (bi)phosphate can adsorb on the electrode surface and hinder the FAOR. In order to gain more intrinsic information on the FAOR on Pd(111), the pH effect of FAOR in solutions in the absence of strongly adsorbed anions has been carried out. KOH is added to maintain the solutions with high pHs. However, as observed in Figure S3, the FAOR current in the negative scan direction is affected by the cations in the solution and the upper potential.[14] For clarity and to diminish the effect of cations, only the j−E curves recorded in the positive scan direction in the SHE scale are displayed in Figure 5. Curves in the RHE scale are also shown in Figure S4. Unlike Au(111)[8,39] and Pt(111)[40] electrodes, the onset potential of FAOR on Pd(111) in alkaline solutions is close to 0.6 V (RHE) and thus is influenced by OH_{ad}. To avoid complications due to the presence of OH_{ad}, the pH effect on the FAOR on Pd(111) in acidic solutions is studied first (Figure 5). Due to the high FAOR activity on Pd(111), the true onset potential is located at potentials more negative than the lower scan potential. It should be recalled that the lower potential is set at 0.2 V to

https://doi.org/10.1021/acscatal.4c02040
ACS Catal. 2024, 14, 8983−8995

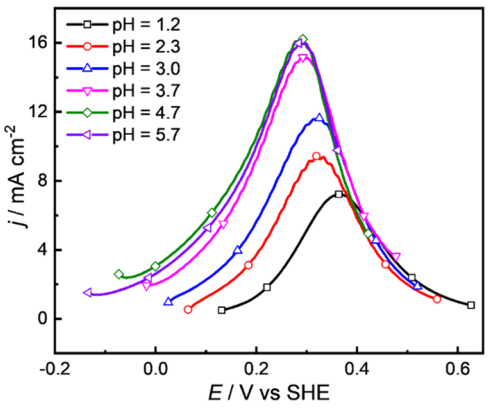

Figure 5. Linear sweep voltammograms in the positive-going scan for FAOR at Pd(111) in 0.1 M HCOOH + 0.1 M $HClO_4$ + x (x < 0.16) M KOH with various pH values, scan rate 50 mV/s. Rotation rate: 1000 rpm.

avoid massive hydrogen absorption on the Pd electrode, which induces surface disordering. Thus, an onset potential cannot be accurately defined. Luckily, the results of ATR-SEIRAS show that adsorbed formate cannot be detected in the potential region before FAOR peak potential.[19] In addition, the CO_2 produced by the reaction is readily transferred from the electrode surface to the bulk solution. Then, it can be proposed that at potentials more negative than the peak potential, the influence of adsorbates in the FAOR is negligible, and a relatively high current for the FAOR (2 mA cm^{-2}) will be used to study the effect of the pH on the onset potential in the SHE scale. As can be seen in Figure 6a, this onset potential of FAOR shifts negatively with a slope of ca. −89 mV with increasing pH when the solution pH is below 4.7. When the pH is higher than 4.7, the onset potential of FAOR remains nearly constant. On the other hand, for potentials above the peak potential, there is no pH effect of the FAOR on Pd(111), that is, the j−E curves in these potentials at different solutions of pHs basically coincide. An explanation for this behavior will be given when the mechanisms are discussed. Additionally, the peak potential shifts negatively with a slope of −27 mV with increasing pH in solutions of pH < 4, and it is constant in the pH range between 4 and 6 (Figure 6a).

Before discussing the possible implication of the pH effect on the FAOR, it must be first ascertained whether the pH effect on the FAOR on Pd(111) is intrinsic or it is due to interference from the reaction-induced shift of interfacial pH^s. Based on the steady-state diffusion layer model under an RDE configuration,[29] the interfacial pH (pH^s) value as a function of the FAOR current is calculated, and it is plotted as a function of the applied potential (Figure 7). Due to the high activity for

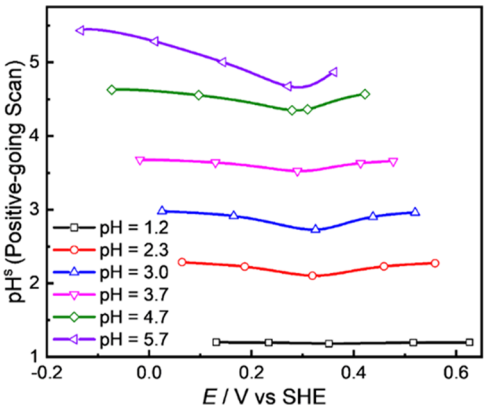

Figure 7. Corresponding interfacial pH^s as a function of the applied potential during FAOR at Pd(111) in solutions with pH lower than 6 calculated based on the model given in ref 29, derived from the original j−E curves recorded in the positive-going scan (Figure 5).

the FAOR on Pd(111), the pH^s drops slightly in the regions with high currents when the solution pH is larger than 2.3. For the solution with pH = 5.7, pH^s drops to ca. 4.7 in the region near the current peak (Figure 7). When those effects are taken into account, the onset and peak potentials for the FAOR can be plotted vs the pH^s (Figure 6b). For the onset potential, the pH dependence after the correction of pH^s shift is nearly the same as that obtained before the correction (Figure 6a). This can be rationalized by the fact that, at these potentials, the FAOR current is too small to cause a significant pH^s shift. In contrast, after the correction of the pH^s-induced shift, the width of FAOR peak plateau decreases. The peak potential plateau in the E-pH^s plots only exists in the range of 3.5 < pH^s < 4.5, instead of 4 < pH^b < 6 before correction.

After studying the FAOR on Pd(111) in acidic solutions, the behavior of the FAOR on the Pd(111) electrode under alkaline conditions was analyzed. Figure 8 displays the linear sweep voltammograms in the positive scan direction for the FAOR at Pd(111) in alkaline conditions. In addition, the interfacial pH (pH^s) is also plotted as a function of the applied potential

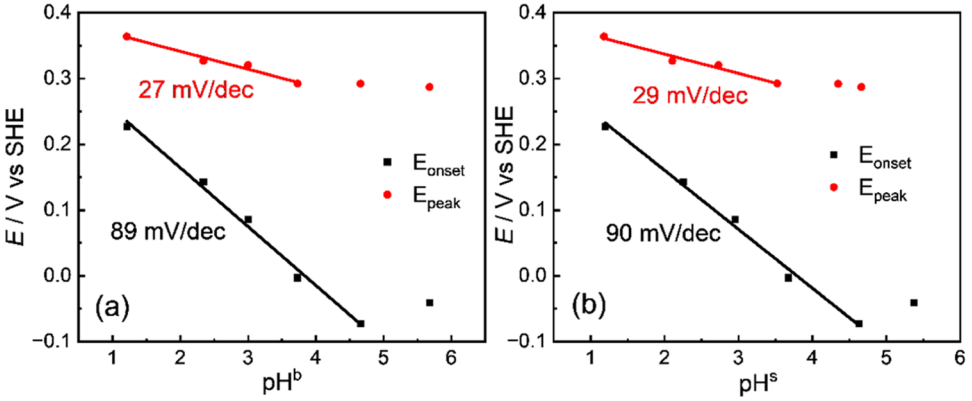

Figure 6. Onset potential and peak potential in SHE scale for FAOR on Pd(111) as a function of solution pH^b (a) from the original data given in Figure 5 or as a function of pH^s (b) after the correction of FAOR-induced drift of interfacial pH^s for the cases with pH within 6.

https://doi.org/10.1021/acscatal.4c02040
ACS Catal. 2024, 14, 8983−8995

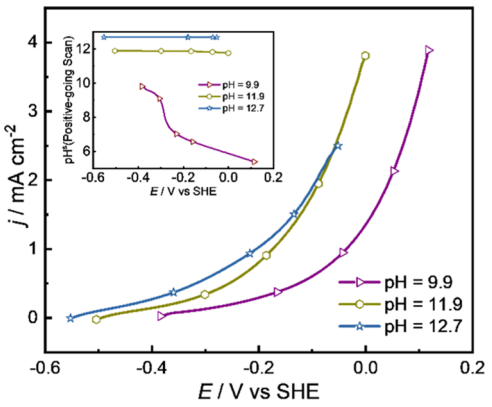

Figure 8. Linear sweep voltammograms in the positive-going scan for FAOR at Pd(111) in 0.1 M HCOOH + 0.1 M $HClO_4$ + x (0.165−0.285) M KOH of various pH values, scan rate 50 mV/s. Rotation rate: 1000 rpm. Inset: corresponding interfacial pH^s as a function of the applied potential during FAOR at Pd(111) in alkaline solutions calculated based on the model given in ref 29, derived from the original j−E curves recorded in the positive-going scan.

based on previous model,[29] as shown in the inset of Figure 8. For pH = 9.9, when the FAOR is occurring, the pH^s drops gradually to ca. 5 with increasing electrode potential, while for solutions with higher pH values, the pH^s on Pd(111) is nearly equal to the bulk pH (pH^b) during the FAOR. Obviously, under alkaline conditions, the FAOR current is severely poisoned by OH_{ad}, even at onset potential. This leads to the current being significantly lower than that in acidic environments. At the same time, in practice, Pd-based catalysts almost all work in acidic conditions. Based on these facts, in the subsequent FAOR mechanism fitting process, only the pH effect on the FAOR on Pd(111) electrodes under acidic conditions will be studied.

The experimental results of the pH effect on the FAOR on Pd(111) in solutions free of strongly adsorbed anions show that (1) In acidic solutions, there is a clear effect of the pH in SHE scale on the FAOR on Pd(111) in potentials lower than the peak. After correcting the pH^s-induced shift, the onset potential of FAOR shifts negatively by ca. −90 mV with increasing pH^s. However, currents after the peak are nearly independent of the pH; (2) In alkaline solutions, the onset potential of FAOR is influenced by OH_{ad}, resulting in lower FAOR currents than that in acidic conditions.

3.1.4. H/D Kinetic Isotope Effect (KIE) for FAOR on Pd(111). To collect more evidence to untangle the mechanism for the FAOR on Pd(111), electrochemical measurements for HCOOH and DCOOH oxidation at Pd(111) in a wide pH range were carried out, (Figure 9). The CVs show an evident decrease in the currents when DCOOH is used. The ratio of the current densities between HCOOH and DCOOH is close to 5, especially near the peak potential (Figure S5), which is consistent with the results on Au(111).[8] This large KIE is probably induced by a primary isotope effect, i.e., the breaking of the C−H/C−D bond in HCOOH/DCOOH is involved in the rate-determining step (RDS) for FAOR on Pd(111). The difference in the rate for the oxidation of HCOOH and DCOOH is probably induced by the differences in the zero-point energy and the transition-state energy of the C−H/C−D bond for HCOOH/DCOOH.[41] The difference in the energy between the transition-state energy and the ground state (zero-point energy) is higher for DCOOH than for HCOOH, i.e., the barrier for splitting the C−D bond is higher than that for the C−H bond. As a result, the oxidation rate for DCOOH is slower than that for HCOOH.[41,42] From our previous analysis, if the C−H/C−D bond is totally broken during the RDS, the theoretical value of the H/D KIE factor should be around 7 for constant potential and reactant concentration in HCOOH and DCOOH solutions.[8,42] In this study, the H/D KIE factors for the FAOR on Pd(111) are ca. 5, which means that, in the transition state, the C−H bond of the reactant is greatly extended (nearly broken). With the increase of pH, the H/D KIE factors are nearly unchanged, suggesting that the degree of extension of the C−H bond in the transition state is the same no matter the solution pH value.

3.2. Mechanistic Discussions of FAOR on Pd(111). Once the electrochemical behavior has been established, it is important to propose a mechanism. Although the electrochemical and spectroscopic results have provided pieces of

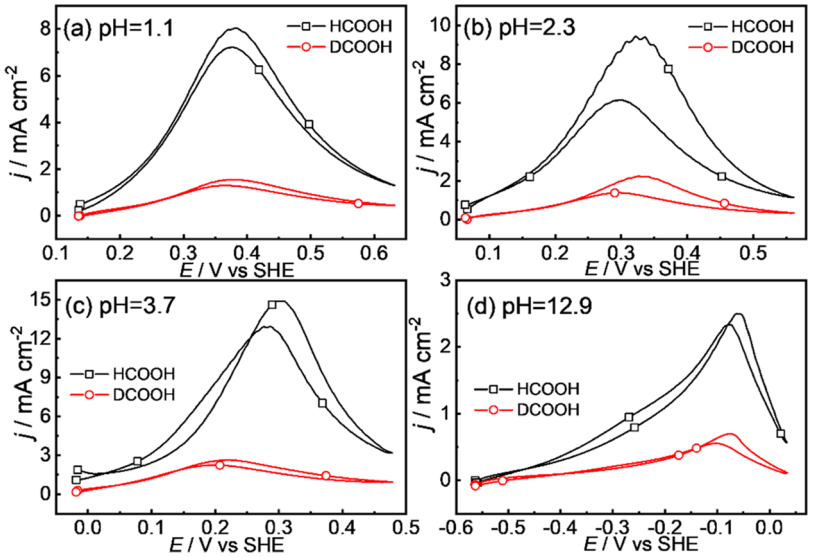

Figure 9. Cyclic voltammograms of FAOR on Pd(111) in 0.1 M $HClO_4$ + 0.1 M HCOOH (square) or DCOOH (circle) + x (0−0.285) M KOH with pH = (a) 1.1, (b) 2.3, (c) 3.7, and (d) 12.9, scan rate: 50 mV/s. Rotation rate: 1000 rpm.

https://doi.org/10.1021/acscatal.4c02040
ACS Catal. 2024, 14, 8983−8995

evidence on the possible steps of this mechanism, there are still some uncertainties regarding the possible intermediates participating in the reaction, so two possible mechanisms will be proposed. Before the discussion of possible mechanisms, the active species for FAOR should be clarified. Based on Figure 5, it is evident that as pH increases within the range of 1.2−3.7, the peak potential shifts toward a more negative value, suggesting rate constant for RDS at FAOR peak potential decreases. However, the peak current density increases with the pH increase within this pH range. This fact implies the concentration of active species should increase as pH increases and the active species for FAOR on Pd(111) are the formate ions.

3.2.1. The Mechanism with $COO_{ad}^{\lambda-}$ as an Intermediate. FAOR is the simplest organic small molecule oxidation reaction involving the transfer of two protons and two electrons. If the RDS of FAOR on Pd(111) is the second step of electron transfer, the product from the first step of electron transfer should accumulate at the electrode interface, which should provide some window to detect it by infrared methods. However, until now no signal related to formate has been observed in the ascending region of the voltammetric currents on the Pd electrode in a solution containing formic acid at pH = 1.[19] This fact suggests that similar to formic acid oxidation on Au(111),[8] the RDS of FAOR on Pd(111) is the step involved first electron transfer. Furthermore, the RDS of the reaction should contain the cleavage of the C−H bond so that the H/D isotope effect can be explained. Considering the competitive adsorption of hydrogen, a possible mechanism of FAOR on Pd(111) should be

$$H_{ad} \rightleftarrows H^+ + e^- + * \quad \text{(R-3)}$$

$$HCOO^- + * \rightleftarrows COO_{ad}^{\lambda-} + H^+ + (2-\lambda)e^- \quad \text{(R-4)}$$

$$COO_{ad}^{\lambda-} \rightleftarrows CO_2 + \lambda e^- + * \quad \text{(R-5)}$$

where "*" stands for a free active site and λ^- is the charge left on the adsorbed $COO_{ad}^{\lambda-}$, whose value is found to be around 1 for the FAOR on Pt(111)[9] and Au(111)[8] electrodes. R-3 reflects the competitive adsorption between H_{ad} and formate. The FAOR on Pd(111) occurs in the potential range of hydrogen adsorption/absorption. Only when hydrogen desorbs from the surface and releases some active sites, formate can adsorb on the electrode surface, and the FAOR occurs. R-4 is the RDS of FAOR on Pd(111) and R-5 is a fast reaction that follows, yielding CO_2 as the final product.

Based on the above analysis, the current density for the FAOR on Pd(111) can be written as

$$j = 2Fk_{4f}c^s_{HCOO^-}\theta_* \quad (3)$$

where k_{4f} is the rate constant of the elementary reaction R-4 in the forward direction. Here, the reverse reaction of R-4 is ignored because of its slow kinetics in the potential range of interest. $c^s_{HCOO^-}$ can be estimated according to eq 4 if the total HCOOH concentration (c_0) is specified.

$$c^s_{HCOO^-} \approx c^b_{HCOO^-} = \frac{c_0}{10^{pK_a - pH^s} + 1} \quad (4)$$

Previous studies suggest when the adsorbate is charged, the effect of electrostatic interaction between the charged adsorbate and the electrode surface cannot be ignored.[8] β_4 is introduced to describe the contribution of electrostatic interaction to the free-energy change of $COO_{ad}^{\lambda-}$ of reaction R-4. So, the rate constant for R-4 can be written as

$$k_{4f} = k_4^0 \exp\left[\frac{\beta_4 F(E - E_4^0)}{RT}\right]\exp\left[\frac{(1-\alpha_4)F(E - E_4^0)}{RT}\right] \quad (5)$$

where k_4^0, E_4^0, and α_4 are the standard rate constant, standard equilibrium potential, and symmetry factor for R-4, respectively. Since the formation of the adsorbate $COO_{ad}^{\lambda-}$ is the RDS of the whole reaction, once $COO_{ad}^{\lambda-}$ is generated, it will be consumed quickly, making its coverage negligible. In the RDE configuration, CO_2 produced by FAOR can be quickly transferred from the interface, so its poison effect is also assumed to be negligible. Although a previous study reveals that no signal related to formate is observed in the ascending region of FAOR current on the Pd electrode,[19] $HCOO_b$ appeared after the peak of the j−E curve of FAOR. Then, it is reasonable to propose that this species is a poison for the FAOR on the Pd electrode. The adsorption of $HCOO_b$ can proceed via the formic acid molecule or formate ion as precursors by the following reactions:

$$HCOOH + 2* \rightleftarrows HCOO_b + H^+ + e^- \quad \text{(R-6)}$$

$$HCOO^- + 2* \rightleftarrows HCOO_b + e^- \quad \text{(R-7)}$$

For the adsorption of $HCOO_b$, its adsorption process should be faster than the desorption process. As an approximation, these reactions R-6, R-7 can be viewed to be in fast quasi-equilibrium. Meanwhile, the dissociation of formic acid ($HCOOH \rightleftarrows HCOO^- + H^+$) is also very fast so that formic acid and formate can be considered to be in equilibrium near the interface. In this case, it is not possible to distinguish the adsorption behaviors of reactions R-6 and R-7. $HCOO^-$ is generally assumed to be the active species in the FAOR process.[43] Then, using R-7, the following expression is obtained:

$$RT\ln c^s_{HCOO^-} + RT\ln\theta_*^n = \gamma_b\theta_b + RT\ln\theta_b - F(E - E_7^0) \quad (6)$$

where E_7^0 is the standard equilibrium potential of reaction R-7; θ_b and θ_* are the coverages of $HCOO_b$ and free sites, which are normalized to the maximum coverage of adsorbates on the electrode, respectively; n is the reaction order of θ_*; and γ_b is the lateral interaction coefficient of $HCOO_b$. For simplicity, it will be assumed that $n = 1$ and that the lateral interactions among adsorbates are negligible, i.e., $\gamma_b = 0$. Then

$$\frac{\theta_b}{\theta_*} = c^s_{HCOO^-}e^{F(E-E_7^0)/RT} \quad (7)$$

At the same time, the FAOR starts in the H-UPD region. Thus, the coverage of H_{ad} should also be considered. If reaction R-3 is assumed to be in a quasi-equilibrium state, the following expression is obtained

$$RT\ln\theta_{H_{ad}} + \gamma_{H_{ad}}\theta_{H_{ad}} = RT\ln c^s_{H^+} + RT\ln\theta_*^n - F(E - E_3^0) \quad (8)$$

where $\gamma_{H_{ad}}$ is the lateral interaction coefficient for H_{ad}. Again, it will be supposed that $n = 1$ and $\gamma_{H_{ad}} = 0$. Thus

https://doi.org/10.1021/acscatal.4c02040
ACS Catal. 2024, 14, 8983−8995

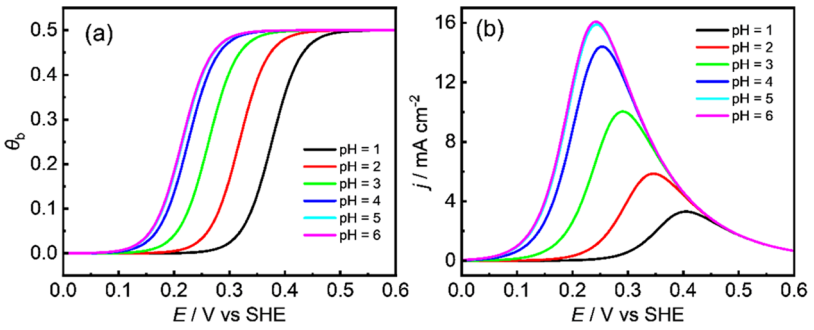

Figure 10. (a) Langmuir adsorption isotherms of $HCOO_b$ at different pHs obtained from eq 12. (b) Simulation results of j–E curves of FAOR on Pd(111) at different pHs derived from eq 13. Parameters selection: E_3^0 = 0 V, E_7^0 = 0.35 V, $k_4^0 = 4.2 \times 10^{-5}$ m/s, α_4 = 0.5, β_4 = 0.25, pK_a = 3.78.

$$\frac{\theta_{H_{ad}}}{\theta_*} = c_{H^+}^s e^{-F(E-E_3^0)/RT} \tag{9}$$

Therefore, the active-sites coverage on the Pd(111) electrode, which can be used for the FAOR under acidic conditions, can be expressed as

$$\theta_* = 1 - \theta_{H_{ad}} - 2\theta_b \tag{10}$$

By combining eqs 7, 9, and 10, the coverages of free sites and $HCOO_b$ can be obtained

$$\theta_* = \frac{1}{1 + c_{H^+}^s e^{-F(E-E_3^0)/RT} + 2c_{HCOO^-}^s e^{F(E-E_7^0)/RT}} \tag{11}$$

$$\theta_b = \frac{2c_{HCOO^-}^s e^{F(E-E_7^0)/RT}}{1 + c_{H^+}^s e^{-F(E-E_3^0)/RT} + 2c_{HCOO^-}^s e^{F(E-E_7^0)/RT}} \tag{12}$$

Substituting eqs 4, 5, and 11 into eq 3, the current of FAOR is

$$j = \frac{2Fk_{4f}c_{HCOO^-}^s}{1 + c_{H^+}^s e^{-F(E-E_3^0)/RT} + 2c_{HCOO^-}^s e^{F(E-E_7^0)/RT}} \tag{13}$$

Equation 12 represents the Langmuir isotherms of $HCOO_b$ adsorption on the Pd(111) electrode under the possible presence of adsorbed H. At the same time, eq 13 also shows a complex j–E curve for the FAOR. After selecting appropriate parameters to match the experimental behavior of the FAOR, the Langmuir adsorption isotherm of $HCOO_b$ and the j–E curve on the Pd(111) electrode under acidic conditions can be obtained (Figure 10). As can be seen in Figure 10a, the coverage of $HCOO_b$ on Pd(111) gradually increases with the increase of electrode potential and finally reaches a stable value. The adsorption isotherms of $HCOO_b$ gradually shift negatively with the increase of pH. When pH > 4, the adsorption isotherms of $HCOO_b$ overlap on the SHE scale. Although the adsorption isotherm of $HCOO_b$ on the Pd(111) electrode cannot be measured because of the high FAOR activity, these curves are similar to the adsorption behavior of CH_3COO_b observed on the Pd(111) electrode.

Figure 10b shows the j–E curve of FAOR on Pd(111) under acidic conditions, which is derived from eq 13. The calculated trend is almost consistent with the experimental results (Figure 5), that is, there is a significant pH effect in the potential range before the peak potential, and when the electrode potential exceeds the peak potential, the pH effect disappears. The j–E behavior agrees qualitatively with the experimental results, which proves the rationality of the mechanism.

Furthermore, the onset potential and peak potential from Figure 10 are plotted vs the pH, as shown in Figure 11. With

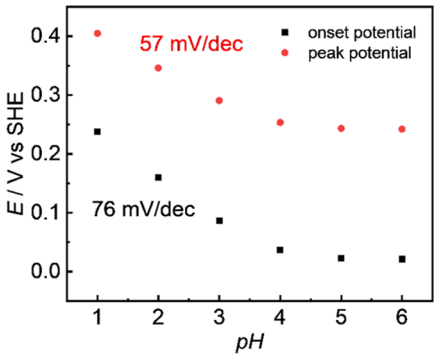

Figure 11. pH dependence of the theoretical FAOR onset potential (corresponding to the current density of 0.1 mA cm^{-2}) and the peak potential obtained from Figure 10b.

the increase of pH, the onset potential of FAOR shows a negative shift of ca. 76 mV per pH unit, which is close to the experimental results. At the same time, the FAOR peak potential also showed a negative shift of ca. 57 mV per pH unit, which is larger than the observation in the experiment. These results indicated that the model does not include all of the relevant parameters. For instance, the adsorption of $HCOO_b$ is assumed to follow a Langmuir isotherm, but lateral interactions can be significant. In the future, further comprehensive consideration and more detailed fitting are needed to reveal other key factors affecting the peak potential here.

Next, the reason for the absence of a pH effect for the FAOR at high potential will be analyzed. After the FAOR peak potential, there is no H_{ad} on the electrode surface, and only $HCOO_b$ poisons the interface. Therefore, by substituting eq 9 into eq 3, the FAOR current density on Pd(111) electrode at high potential is

$$j = 2Fk_{4f}\theta_b e^{-F(E-E_7^0)/RT} \tag{14}$$

As can be seen from eq 14, when θ_b is constant, FAOR currents in different pH values are the same under the same electrode potential. It can also be found from Figure 10 that in the potential range where the FAOR currents overlap at high potentials, the coverage of $HCOO_b$ is constant, which is consistent with the inference of eq 14. Therefore, the reason for the absence of a pH effect on the FAOR at high potentials is that the coverage of $HCOO_b$ at these high potentials reaches its maximum coverage.

https://doi.org/10.1021/acscatal.4c02040
ACS Catal. 2024, 14, 8983−8995

Although it is impossible to measure the coverage of $HCOO_b$ on Pd(111), the behavior of acetic acid can be used as an analogy.[8,38] From the inset of Figure S2, the maximum coverages of CH_3COO_b in higher electrode potentials are ca. 0.26 ML in the solutions of pH < 6, so it can be assumed that the coverage of $HCOO_b$ is also almost constant at high potentials. This fact results in almost consistent FAOR currents at high potentials in solutions with different pH values, as predicted from eq 14.

3.2.2. The Mechanism with $HCOO_m$ as an Intermediate. The PZC of Pd(111) in 0.1 M $HClO_4$ is about 0.22 V_{SHE},[15] and on the SHE scale, PZC does not change with pH. From this view, as shown in Figure 5, a large FAOR current has been generated on the Pd(111) electrodes with a negative charge. Under these circumstances, the formation of a negatively charged species, $COO_{ad}^{\lambda-}$, seems to be difficult, which may hinder the previously proposed mechanism. Therefore, another direct FAOR mechanism may operate in the low-potential region. Studies of the FAOR on Pt(111)[9,43] have proposed the monodentate adsorbed formate ($HCOO_m$) as the intermediate in the reaction. Since the FAOR on Pd(111) has a large Tafel slope at low potential (as shown in Figure 1), the RDS cannot be the second electron transfer. It should be the first electron transfer step or the chemical step after the first electron transfer. Also, to satisfy the large H/D KIE factor observed experimentally (Figure 9), the RDS must be involved in the breaking of the C−H bond. Thus, a possible mechanism is

$$H_{ad} \rightleftarrows H^+ + e^- + * \quad \text{(R-3)}$$

$$HCOO^- + * \rightleftarrows HCOO_m + e^- \quad \text{(R-8)}$$

$$HCOO_m \rightleftarrows CO_2 + H_{ad} \quad \text{(R-9)}$$

The last step in the mechanism is then the desorption of the H_{ad} and the transfer of the second electron (R-3). Based on the above facts, R-9 should be the RDS for this mechanism. It should be noted that at the onset potential for the FAOR, H_{ad} is a stable species here, which serves as a strongly bonded intermediate in the mechanism proposed earlier,[16,44] and thus, its coverage is determined by the adsorption isotherm. For this mechanism, the current density of FAOR on Pd(111) can be expressed as

$$j = 2Fk_{9f}\theta_m \quad (15)$$

where k_{9f} is the reaction rate constant of the forward reaction of R-9 and θ_m is the coverage of $HCOO_m$. The free-sites coverage on the surface of the Pd(111) electrode under acidic environments should take into account the sites occupied by H_{ad}, $HCOO_m$, and $HCOO_b$, according to

$$\theta_* = 1 - \theta_{H_{ad}} - 2\theta_b - \theta_m \quad (16)$$

When R-8 is assumed to be in a quasi-equilibrium state, a relationship between θ_m and θ_* can be obtained

$$RT \ln c^s_{HCOO^-} + RT \ln \theta_*^n = \gamma_m\theta_m + RT \ln \theta_m - F(E - E_8^0) \quad (17)$$

where γ_m is the lateral interaction coefficient for $HCOO_m$. For simplicity, it is assumed that $n = 1$ and the lateral interaction among adsorbates is negligible, i.e., $\gamma_m = 0$. Thus

$$\frac{\theta_m}{\theta_*} = c^s_{HCOO^-} e^{F(E-E_8^0)/RT} \quad (18)$$

By combining eqs 7, 9, 16, and 18, the coverage of $HCOO_m$ is

$$\theta_m = \left[c^s_{HCOO^-} e^{F(E-E_8^0)/RT}\right] \Big/ \left[1 + c^s_{H^+} e^{-F(E-E_3^0)/RT} + 2c^s_{HCOO^-} e^{F(E-E_7^0)/RT} + c^s_{HCOO^-} e^{F(E-E_8^0)/RT}\right] \quad (19)$$

And then, the FAOR current density on Pd(111) is

$$j = \left[2Fk_{9f}c^s_{HCOO^-} e^{F(E-E_8^0)/RT}\right] \Big/ \left[1 + c^s_{H^+} e^{-F(E-E_3^0)/RT} + 2c^s_{HCOO^-} e^{F(E-E_7^0)/RT} + c^s_{HCOO^-} e^{F(E-E_8^0)/RT}\right] \quad (20)$$

Here, k_{9f} is a rate constant of a chemical reaction, which is independent of the electrode potential. Using this expression with appropriate values for the parameters, $j-E$ curves were obtained, as shown in Figure 12.

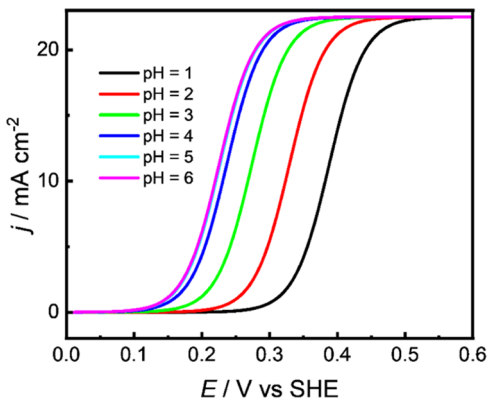

Figure 12. Simulation results of $j-E$ curves of FAOR on Pd(111) at different pHs derived from eq 20. Parameters selection: E_3^0 = 0 V, E_7^0 = 0.4 V, E_8^0 = 0.35 V, $k_9^0 = 1.5 \times 10^{-3}$ m/s, pK_a = 3.78.

Using this expression, a peak in the j vs E plot is not obtained and after a given potential, the current is constant. This constant current is the result of the two opposing effects: the increase of $HCOO_m$ adsorption strength (R-8) with the potential and the diminution of the free sites due to the formation of a full layer of $HCOO_b$, which inhibits the reaction. Since the potential dependence of both processes is the same (with opposed signs), the result is a constant current. However, if there is a repulsive interaction between adsorbates, reaction R-8 would be further inhibited at high $HCOO_b$ coverages, resulting in a smaller increase of the $HCOO_m$ adsorption strength. On the other hand, at lower potentials, the pH dependence of the FAOR onset potential is similar to the experimental results (Figure 5), indicating that the mechanism may still be feasible at lower potentials. Furthermore, the calculated FAOR onset potential in solutions was plotted vs the pH (Figure 13). It is obvious that with the increase of pH, the FAOR onset potential shows a negative shift of ca. 57 mV per pH unit, which is lower than the experimental result (90 mV per pH unit). It should be noted that this value depends on the actual H_{ad} coverage. In the simulation, it has been assumed that this process follows a Langmuir isotherm. However, the shape of the hydrogen adsorption region is that expected for a process following a Frumkin isotherm with repulsive interactions.

At the same time, this mechanism also has obvious defects. In this mechanism, if R-9 is the RDS, then the fast reaction R-8 must cause the $HCOO_m$ to accumulate at the electrode

https://doi.org/10.1021/acscatal.4c02040
ACS Catal. 2024, 14, 8983−8995

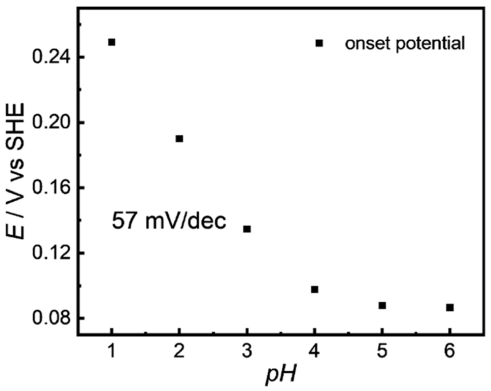

Figure 13. pH dependence of the theoretical FAOR onset potential (corresponding to the current density of 0.1 mA cm^{-2}) obtained from Figure 12.

interface. According to the previous hypothesis, $HCOO_m$ and $HCOO_b$ at the electrode interface can be converted into each other[43]

$$* + HCOO_m \rightleftarrows HCOO_b \quad \text{(R-10)}$$

If so, the presence of $HCOO_b$ on the electrode interface should be observed by IR. However, the actual situation is that in the FAOR current rising region of Pd(111), no $HCOO_b$ signal can be observed through IR.[19] However, due to its pH dependence of onset potential at low potential similar to the experimental results, we still cannot completely rule out the possibility of this pathway with $HCOO_m$ consumption as RDS.

In summary, for the mechanisms of FAOR on Pd(111), both the HCOO pathway with $HCOO_m$ consumption as the RDS and the COO pathway with $COO_{ad}^{\lambda-}$ generation as the RDS may exist in the potential region before the FAOR peak potential. Given the uncertainties of the lateral interaction coefficient for both the adsorbed species, none of those mechanisms can be ruled out. For these two possible mechanisms under low potential, some phenomena are difficult to explain. For the COO pathway, at the negatively charged electrode interface, why can the negatively charged active intermediate $COO_{ad}^{\lambda-}$ adsorb at the electrode interface? Possible reasons could include the adsorption of hydrogen causing a shift in the PZC. The adsorption of hydrogen, along with the number of surface water molecules affected by its coverage, could lead to changes in dipole moments. The changes in dipoles and their impact on the extent of surface electron spillover can result in alterations to the PZC. It needs to be further proved. For the HCOO pathway, since the RDS is the consumption of the active intermediate, formate species must accumulate at the electrode interface, and its coverage should be large enough to be detected by spectroscopic techniques. However, so far, no signal related to formate has been observed on the Pd electrode surface in the FAOR current rising region. In the future, it is necessary to improve the temporal and spatial resolution of spectral techniques to provide a technical basis for the detection of FAOR active intermediates and to clarify the possibility and contribution of these two channels.

4. CONCLUSIONS

The pH effect and H/D kinetic isotope effect of FAOR on Pd(111) have been studied by cyclic voltammetry. In addition, the pH effect of acetate adsorption on Pd(111) is further studied to gain insight into the roles of adsorbates during FAOR on Pd(111). The experimental results show that (1) In solutions with the same total acetic acid concentration, at pH < pK_a of acetic acid, the onset potential of acetate desorption is almost unchanged with increasing pH on the RHE scale. When pH is higher than the pK_a of acetic acid, the onset potential of acetate desorption shifted positively with a slope of ca. 20 mV per pH unit; (2) In solutions with pH less than 6, the maximum coverage of acetate adsorbed on the Pd(111) electrode is about 0.26 ML; (3) In acidic solutions, the solution pH has a significant effect on the FAOR on Pd(111). After correcting the pH^s-induced shift, the onset potential of FAOR shifts negatively by ca. 90 mV per pH unit. However, the pH effect disappears in the potential range of current decreasing; (4) In alkaline solutions, the onset potential of FAOR is influenced by OH_{ad}; (5) The H/D kinetic isotope effect factor of FAOR on Pd(111) is ca. 5 in the pH range of 1−14.

Simulation results show the pathway with $COO_{ad}^{\lambda-}$ generation as the rate-determining step (COO pathway) and the pathway with $HCOO_m$ consumption as the rate-determining step (HCOO pathway) could be the main direct pathways of FAOR on Pd(111) in the potential region before the peak potential. After the peak potential, due to the positive charge on the surface of Pd(111), the COO pathway dominates. The reason why there is no pH effect after FAOR peak potential is that the $HCOO_b$ coverage on Pd(111) in these potentials at different pH values is constant and inhibits the reaction.

■ ASSOCIATED CONTENT

Supporting Information

The following files are available free of charge. The Supporting Information is available free of charge at https://pubs.acs.org/doi/10.1021/acscatal.4c02040.

Calculations of the interfacial pH; CVs of Pd(111) in solutions with different anions in a high scan rate; calculations of the maximum coverages of acetate adsorption in solutions with pH < 6; influence of cations and upper potentials for FAOR on Pd(111); pH effect for FAOR on Pd(111) in the RHE scale; and potential-dependent H/D KIE factors for FAOR on Pd(111) (PDF)

■ AUTHOR INFORMATION

Corresponding Authors

Yan-Xia Chen − *Hefei National Research Center for Physical Sciences at Microscale, Department of Chemical Physics, University of Science and Technology of China, Hefei 230026, China;* orcid.org/0000-0002-1370-7422; Email: yachen@ustc.edu.cn

Enrique Herrero − *Instituto de Electroquímica, Universidad de Alicante, E-03080 Alicante, Spain;* orcid.org/0000-0002-4509-9716; Email: herrero@ua.es

Authors

Zhen Wei − *Hefei National Research Center for Physical Sciences at Microscale, Department of Chemical Physics, University of Science and Technology of China, Hefei 230026, China; Instituto de Electroquímica, Universidad de Alicante, E-03080 Alicante, Spain*

https://doi.org/10.1021/acscatal.4c02040
ACS Catal. 2024, 14, 8983−8995

Meng-Ke Zhang − *Hefei National Research Center for Physical Sciences at Microscale, Department of Chemical Physics, University of Science and Technology of China, Hefei 230026, China*

Yan-Hao Yu − *Hefei National Research Center for Physical Sciences at Microscale, Department of Chemical Physics, University of Science and Technology of China, Hefei 230026, China*

Jun Cai − *Hefei National Research Center for Physical Sciences at Microscale, Department of Chemical Physics, University of Science and Technology of China, Hefei 230026, China*

Juan M. Feliu − *Instituto de Electroquímica, Universidad de Alicante, E-03080 Alicante, Spain;* orcid.org/0000-0003-4751-3279

Complete contact information is available at: https://pubs.acs.org/10.1021/acscatal.4c02040

Author Contributions

[§]Z.W. and M.-K.Z. contributed equally to this work. The manuscript was written through contributions of all authors. All authors have given approval to the final version of the manuscript.

Funding

This work was financially supported by the National Natural Science Foundation of China (nos. 22172151 and 22372154). E.H. and J.M.F. acknowledge financial support from Ministerio de Ciencia, Innovación y Universidades (Project PID2022-137350NB-I00). Zhen Wei acknowledges support from the China Scholarship Council (award number 202106340060).

Notes

The authors declare no competing financial interest.

■ ABBREVIATIONS

FAOR, formic acid oxidation reaction
CV, cyclic voltammograms
RHE, reversible hydrogen electrode
SHE, standard hydrogen electrode
PZC, potential of zero charge

■ REFERENCES

(1) Chen, X.; Granda-Marulanda, L. P.; McCrum, I. T.; Koper, M. T. M. How palladium inhibits CO poisoning during electrocatalytic formic acid oxidation and carbon dioxide reduction. *Nat. Commun.* **2022**, *13* (1), No. 38.

(2) Mekazni, D. S.; Arán-Ais, R. M.; Herrero, E.; Feliu, J. M. On the oxidation of isopropanol on platinum single crystal electrodes. A detailed voltammetric and FTIR study. *J. Power Sources* **2023**, *556*, No. 232396.

(3) Mekazni, D. S.; Arán-Ais, R. M.; Ferre-Vilaplana, A.; Herrero, E. Why Methanol Electro-oxidation on Platinum in Water Takes Place Only in the Presence of Adsorbed OH. *ACS Catal.* **2022**, *12* (3), 1965−1970.

(4) Wei, Z.; Yu, A.; Gisbert-González, J. M.; Cai, J.; Chen, Y.-X.; Feliu, J. M.; Herrero, E. Mechanism of formic acid oxidation on Bi modified Pt(111): Implication from the concentration effect of formic acid and different coverages of Bi. *Electrochim. Acta* **2023**, *449*, No. 142188.

(5) Wei, Z.; Jordá-Faus, P.; Chico-Mesa, L.; Cai, J.; Chen, Y.-X.; Rodes, A.; Feliu, J. M.; Herrero, E. Formic acid oxidation on different coverages of Bismuth-modified Pt(100): A detailed voltammetric and FTIR study. *J. Catal.* **2023**, *426*, 61−70.

(6) Rizo, R.; Arán-Ais, R. M.; Herrero, E. On the oxidation mechanism of C1-C2 organic molecules on platinum. A comparative analysis. *Curr. Opin. Electrochem.* **2021**, *25*, 100648.

(7) Koper, M. T. M.; Lai, S. C. S.; Herrero, E. Mechanisms of the Oxidation of Carbon Monoxide and Small Organic Molecules at Metal Electrodes. *Fuel Cell Catal.* **2009**, 159−207.

(8) Wei, Z.; Zhang, M. K.; Zhu, B. Q.; Cai, J.; Chen, Y.-X. Mechanistic Insight into Formic Acid/Formate Oxidation at the Au(111) Electrode: Implications from the pH Effect and H/D Kinetic Isotope Effect. *J. Phys. Chem. C* **2022**, *126* (29), 11987−12002.

(9) Zhang, M.-K.; Chen, W.; Wei, Z.; Xu, M.-L.; He, Z.; Cai, J.; Chen, Y.-X.; Santos, E. Mechanistic Implication of the pH Effect and H/D Kinetic Isotope Effect on HCOOH/HCOO$^-$ Oxidation at Pt Electrodes: A Study by Computer Simulation. *ACS Catal.* **2021**, *11* (12), 6920−6930.

(10) Joo, J.; Uchida, T.; Cuesta, A.; Koper, M. T. M.; Osawa, M. Importance of Acid−Base Equilibrium in Electrocatalytic Oxidation of Formic Acid on Platinum. *J. Am. Chem. Soc.* **2013**, *135* (27), 9991−9994.

(11) Jiang, K.; Zhang, H.-X.; Zou, S.; Cai, W.-B. Electrocatalysis of formic acid on palladium and platinum surfaces: from fundamental mechanisms to fuel cell applications. *Phys. Chem. Chem. Phys.* **2014**, *16* (38), 20360−20376.

(12) Betts, A.; Briega-Martos, V.; Cuesta, A.; Herrero, E. Adsorbed Formate is the Last Common Intermediate in the Dual-Path Mechanism of the Electrooxidation of Formic Acid. *ACS Catal.* **2020**, *10* (15), 8120−8130.

(13) Capon, A.; Parsons, R. The oxidation of formic acid on noble metal electrodes: II. A comparison of the behaviour of pure electrodes. *J. Electroanal. Chem. Interfacial Electrochem.* **1973**, *44* (2), 239−254.

(14) Lei, J.; Wei, Z.; Xu, M.-l.; Wei, J.; Chen, Y.-x.; Ye, S. Effect of sulfate adlayer on formic acid oxidation on Pd(111) electrode. *Chin. J. Chem. Phys.* **2019**, *32* (6), 649−656.

(15) Hara, M.; Linke, U.; Wandlowski, T. Preparation and electrochemical characterization of palladium single crystal electrodes in 0.1 M H_2SO_4 and $HClO_4$: Part I. Low-index phases. *Electrochim. Acta* **2007**, *52* (18), 5733−5748.

(16) Montero, M. A.; Luque, G. C.; Gennero de Chialvo, M. R.; Chialvo, A. C. Kinetic evaluation of the formic acid electrooxidation on steady state on palladium using a flow cell. *J. Electroanal. Chem.* **2020**, *879*, 114777.

(17) Rizo, R.; Roldan Cuenya, B. Shape-Controlled Nanoparticles as Anodic Catalysts in Low-Temperature Fuel Cells. *ACS Energy Lett.* **2019**, *4* (6), 1484−1495.

(18) Haan, J. L.; Masel, R. I. The influence of solution pH on rates of an electrocatalytic reaction: Formic acid electrooxidation on platinum and palladium. *Electrochim. Acta* **2009**, *54* (16), 4073−4078.

(19) Miyake, H.; Okada, T.; Samjeské, G.; Osawa, M. Formic acid electrooxidation on Pd in acidic solutions studied by surface-enhanced infrared absorption spectroscopy. *Phys. Chem. Chem. Phys.* **2008**, *10* (25), 3662−3669.

(20) Hoshi, N.; Kida, K.; Nakamura, M.; Nakada, M.; Osada, K. Structural Effects of Electrochemical Oxidation of Formic Acid on Single Crystal Electrodes of Palladium. *J. Phys. Chem. B* **2006**, *110* (25), 12480−12484.

(21) Hoshi, N.; Nakamura, M.; Kida, K. Structural effects on the oxidation of formic acid on the high index planes of palladium. *Electrochem. Commun.* **2007**, *9* (2), 279−282.

(22) Vidal-Iglesias, F. J.; Solla-Gullón, J.; Herrero, E.; Aldaz, A.; Feliu, J. M. Formic acid oxidation on Pd-modified Pt(100) and Pt(111) electrodes: A DEMS study. *J. Appl. Electrochem.* **2006**, *36* (11), 1207−1214.

(23) Chen, X.; Granda-Marulanda, L. P.; McCrum, I. T.; Koper, M. T. M. Adsorption processes on a Pd monolayer-modified Pt(111) electrode. *Chem. Sci.* **2020**, *11* (6), 1703−1713.

(24) Baldauf, M.; Kolb, D. M. Formic Acid Oxidation on Ultrathin Pd Films on Au(hkl) and Pt(hkl) Electrodes. *J. Phys. Chem. A* **1996**, *100* (27), 11375−11381.

(25) Uwitonze, N.; Zhou, D.; Lei, J.; Chen, W.; Zuo, X. Q.; Cai, J.; Chen, Y.-X. The high Tafel slope and small potential dependence of

activation energy for formic acid oxidation on a Pd electrode. *Electrochim. Acta* **2018**, *283*, 1213−1222.
(26) Shi, Y.; Schimmenti, R.; Zhu, S.; Venkatraman, K.; Chen, R.; Chi, M.; Shao, M.; Mavrikakis, M.; Xia, Y. Solution-Phase Synthesis of $PdH_{0.706}$ Nanocubes with Enhanced Stability and Activity toward Formic Acid Oxidation. *J. Am. Chem. Soc.* **2022**, *144* (6), 2556−2568.
(27) Clavilier, J.; Faure, R.; Guinet, G.; Durand, R. Preparation of monocrystalline Pt microelectrodes and electrochemical study of the plane surfaces cut in the direction of the {111} and {110} planes. *J. Electroanal. Chem. Interfacial Electrochem.* **1980**, *107* (1), 205−209.
(28) Cuesta, A.; Kibler, L. A.; Kolb, D. M. A method to prepare single crystal electrodes of reactive metals: application to Pd(hkl). *J. Electroanal. Chem.* **1999**, *466* (2), 165−168.
(29) Zhang, M.-K.; Wei, Z.; Chen, W.; Xu, M.-L.; Cai, J.; Chen, Y.-X. Bell shape vs volcano shape pH dependent kinetics of the electrochemical oxidation of formic acid and formate, intrinsic kinetics or local pH shift? *Electrochim. Acta* **2020**, *363*, No. 137160.
(30) Wei, Z.; Zhang, M. K.; Zhu, B. Q.; Xu, M. L.; Lei, J.; Tang, H.; Cai, J.; Chen, Y.-X. Effect of pH on Sulfate Adsorption on the Pd(111) Electrode. *J. Phys. Chem. C* **2022**, *126* (8), 3891−3902.
(31) Solomun, T. Initial stages of electrooxidation of Pd (100) surfaces in sulfuric acid solution: An XPS study. *J. Electroanal. Chem. Interfacial Electrochem.* **1987**, *217* (2), 435−441.
(32) Solomun, T. Electro-oxidation of the Pd (100) surface: Potential dependence of oxygen incorporation into the substrate. *J. Electroanal. Chem. Interfacial Electrochem.* **1988**, *255* (1), 163−177.
(33) Samjeské, G.; Miki, A.; Ye, S.; Osawa, M. Mechanistic Study of Electrocatalytic Oxidation of Formic Acid at Platinum in Acidic Solution by Time-Resolved Surface-Enhanced Infrared Absorption Spectroscopy. *J. Phys. Chem. B* **2006**, *110* (33), 16559−16566.
(34) Miki, A.; Ye, S.; Senzaki, T.; Osawa, M. Surface-enhanced infrared study of catalytic electrooxidation of formaldehyde, methyl formate, and dimethoxymethane on platinum electrodes in acidic solution. *J. Electroanal. Chem.* **2004**, *563* (1), 23−31.
(35) Samjeské, G.; Miki, A.; Osawa, M. Electrocatalytic Oxidation of Formaldehyde on Platinum under Galvanostatic and Potential Sweep Conditions Studied by Time-Resolved Surface-Enhanced Infrared Spectroscopy. *J. Phys. Chem. C* **2007**, *111* (41), 15074−15083.
(36) Wang, J.-Y.; Zhang, H.-X.; Jiang, K.; Cai, W.-B. From HCOOH to CO at Pd Electrodes: A Surface-Enhanced Infrared Spectroscopy Study. *J. Am. Chem. Soc.* **2011**, *133* (38), 14876−14879.
(37) Zuo, X. Q.; Chen, W.; Yu, A.; Le Xu, M.; Cai, J.; Chen, Y.-X. pH effect on acetate adsorption at Pt(111) electrode. *Electrochem. Commun.* **2018**, *89*, 6−9.
(38) Abdelrahman, A.; Hermann, J. M.; Jacob, T.; Kibler, L. A. Adsorption of Acetate on Au(111): An in-situ Scanning Tunnelling Microscopy Study and Implications on Formic Acid Electrooxidation. *ChemPhysChem* **2019**, *20* (22), 2989−2996.
(39) Hermann, J. M.; Abdelrahman, A.; Jacob, T.; Kibler, L. A. The Effect of pH and Anion Adsorption on Formic Acid Oxidation on Au(111) Electrodes. *Electrochim. Acta* **2021**, *385*, No. 138279.
(40) Ferre-Vilaplana, A.; Perales-Rondón, J. V.; Buso-Rogero, C.; Feliu, J. M.; Herrero, E. Formic acid oxidation on platinum electrodes: a detailed mechanism supported by experiments and calculations on well-defined surfaces. *J. Mater. Chem. A* **2017**, *5* (41), 21773−21784.
(41) Chen, Y.-X.; Heinen, M.; Jusys, Z.; Behm, R. J. Kinetic Isotope Effects in Complex Reaction Networks: Formic Acid Electro-Oxidation. *ChemPhysChem* **2007**, *8* (3), 380−385.
(42) Wei, Y.; Zuo, X. Q.; He, Z. D.; Chen, W.; Lin, C. H.; Cai, J.; Sartin, M.; Chen, Y.-X. The mechanisms of $HCOOH/HCOO^-$ oxidation on Pt electrodes: Implication from the pH effect and H/D kinetic isotope effect. *Electrochem. Commun.* **2017**, *81*, 1−4.
(43) Salamon, M. J.; Briega-Martos, V.; Cuesta, A.; Herrero, E. Insight into the role of adsorbed formate in the oxidation of formic acid from pH-dependent experiments with Pt single-crystal electrodes. *J. Electroanal. Chem.* **2022**, *925*, 116886.
(44) Luque, G. C.; de Chialvo, M. R. G.; Chialvo, A. C. Influence of spontaneous decomposition on the electrochemical formic acid oxidation on a nanostructured palladium electrode. *Electrochem. Commun.* **2016**, *70*, 69−72.

https://doi.org/10.1021/acscatal.4c02040
ACS Catal. 2024, 14, 8983−8995